Phase-space structure of a thermoreceptor

Wolfgang Braun,[1] Bruno Eckhardt,[1] Hans A. Braun,[2] and Martin Huber[3]
[1]*Fachbereich Physik, Philipps Universität Marburg, D-35037 Marburg, Germany*
[2]*Institut für Physiologie, Philipps Universität Marburg, D-35033 Marburg, Germany*
[3]*Klinik für Psychiatrie, Philipps Universität Marburg, D-35032 Marburg, Germany*
(Received 4 June 1999; revised manuscript received 13 July 2000)

We analyze the phase-space structure of a model for thermoreceptors in fish and mammals. As a function of the temperature we identify a period doubling scenario at low temperatures, a regime where an unstable stationary fixed point collides with the attractor and blocks the thermoreceptor, and a transition from period $n+1$ to period n as the temperature is further increased. The period reduction phenomenon is due to an autoresonance between fast and slow ion channels and shows the features typical for mode locking.

PACS number(s): 05.45.Ac, 05.45.Tp, 87.19.La, 87.19.Nn

I. INTRODUCTION

Sensory neurons translate continuous input into spike trains which are transmitted along axons to other neurons that process the information further. The response of sensory receptors in fish [1,2] and mammals [3,4] to various stimuli (electrical, thermal, sharp transition or gradual transition) has been studied in a series of experiments by Braun *et al.* The relation between temperature change and impulse patterns was found not to be monotonic, but to be influenced by nonlinear and chaotic responses of the sensor as well as noise in the system. Typical impulse patterns show regular single spike activity and rhythmic groupings of spikes into bursts as well as irregular activity with multimodal spike interval distributions. The experiments have stimulated the development of methods to identify signatures of chaos in signals with a considerable amount of noise, and specific methods to extract periodic orbits have been proposed [5]. Motivated by these investigations and the existence of a model [6] that can account for most observed features in the temperature dependent changes of cold receptor activity, we here propose an analysis of the model from a nonlinear dynamics point of view.

The cold receptor model has four dynamically active degrees of freedom, and is thus capable of nontrivial and potentially chaotic dynamics. The external parameter is the temperature, the measured signal the interval between spikes in the voltage across the cell membrane. The details of the model will be given in the next section. The model is designed to describe temperature dependent changes of the impulse patterns. Figure 1 compares experimental data and data from the model with a certain amount of noise added. For most of the temperature range shown noise leads just to a smearing of interspike intervals. However, for high temperatures the noise is responsible for occasional skipping of spike formation. This multimodal interspike interval distribution in the upper temperature range can only be reproduced with noise.

Our focus here is on the dynamics without noise, where the model produces the interspike intervals shown in Fig. 2 for slowly increasing (top) and decreasing (bottom) temperature. While this looks on first sight like the usual bifurcation diagram there are a number of conspicuous features on which we would like to focus in the following. First, there are some differences between the two diagrams (marked by the label A): The points where the period 2 orbits split off and where they coalesce, respectively, are different and the shape of the curve is not square-root-like, as expected for the period doubling scenario. Second, for higher temperatures (B) the maximum of the interspike interval increases and no upper limit is recognizable. The absence of an upper limit means that the spike encoder ceases to function. Third, the dynamics in this temperature range is largely chaotic but with a clear accumulation of interspike intervals near two values, the lower one being close to 150 ms and the upper one decreasing from about 1000 ms at 8 °C to 650 ms near 13 °C (indicated by the label C). At slightly higher temperatures strongly hysteretic differences in behavior between increasing and decreasing temperatures can be observed (D). A fourth and perhaps most interesting observation is the transition from period $n+1$ to period n behavior when increasing the temperature from about 15 °C upward (E,F,G).

We here want to study the above mentioned features from the vantage point of dynamical system theory [7,8]. We search for periodic orbits, calculate their stability, and follow

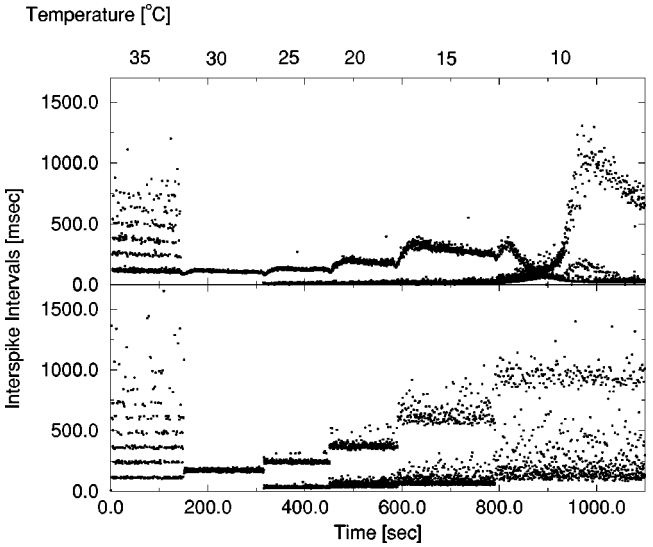

FIG. 1. Experimental data from a peripheral cold receptor of cats (top) and data from the model with additive noise (bottom).

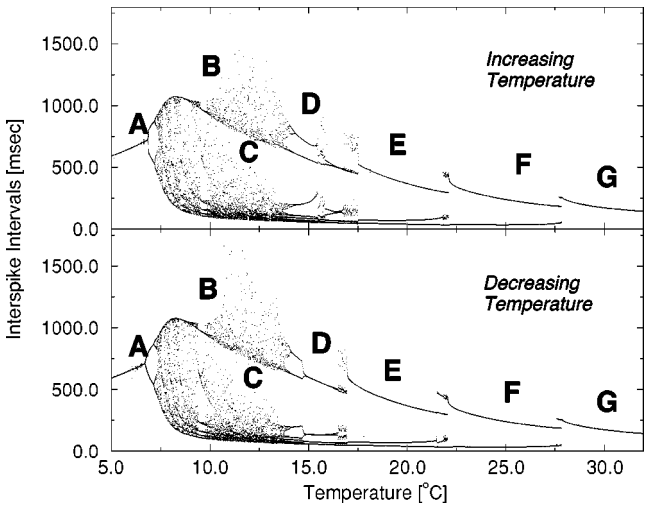

FIG. 2. Interspike intervals for increasing (top) and decreasing (bottom) temperature. The plots were obtained by changing the temperature by 0.0015 °C after every spike. This corresponds to a temperature gradient of about ±0.003 °C/ms. The labels A–G point to the various features discussed in the text.

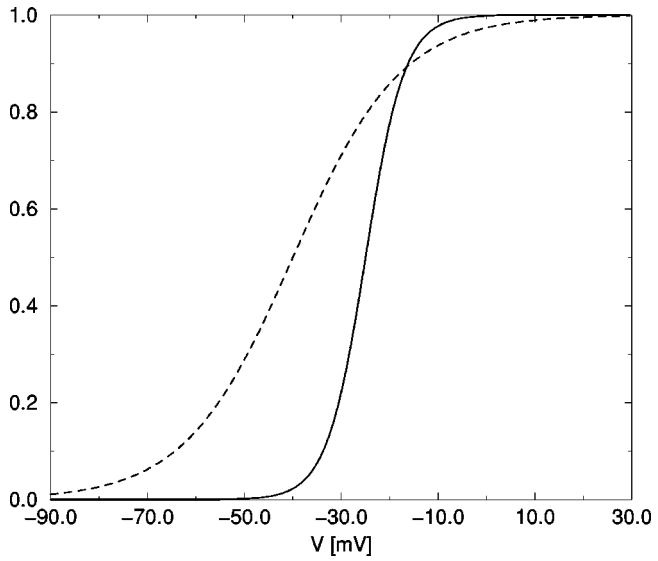

FIG. 3. Equilibrium states of the activation curves for the fast ion channels ($a_{\mathrm{Na}}=a_{\mathrm{K},\infty}$, solid line) and the polarization channels ($a_{sd,\infty}$, dashed line).

their development under changes of parameters. As will be shown, this allows us to explain the dynamical response of the system rather well. In particular, we can connect the four observations mentioned above to the sweeping of a period doubling bifurcation, the presence of an unstable fixed point, the shape of the return map, and an autoresonance between fast and slow ion channels, respectively.

The outline of the paper is as follows. In the next section we describe the model and the numerical methods. This is followed by a discussion of the period doubling scenario (Sec. III), the divergence of the interspike intervals (Sec. IV), and the accumulation of points (Sec. V). Finally, we address the period decreasing transitions for higher temperatures in Sec. VI. In a concluding section we discuss the physiological relevance of the various phase-space features found here.

II. MODEL AND NUMERICAL METHODS

The model for the thermoreceptors is based on the Hodgkin-Huxley model [9]. It uses a simplified version of the classical spike-generating conductances (e.g., without inactivation) but is extended for two additional slow channels activated at lower potentials to account for slow subthreshold potential oscillations which are assumed to underlie the slow rhythms of impulse generation. A temperature dependence is introduced mainly by scaling of the rate constants and, to a lesser extent, by scaling of the maximum conductances.

The principal observable is the potential difference V (measured in millivolts) across the membrane, which is controlled by five currents according to

$$C_M \frac{dV}{dt} = -I_{\mathrm{Na}} - I_{\mathrm{K}} - I_{sd} - I_{sr} - I_l, \tag{1}$$

where C_M is the capacitance of the membrane. The currents on the right hand side fall into three groups. The first two, I_{Na} and I_{K}, are the fast sodium and potassium currents that generate the action potentials,

$$I_{\mathrm{Na}} = \rho g_{\mathrm{Na}} a_{\mathrm{Na}} (V - V_{\mathrm{Na}}), \tag{2}$$

$$I_K = \rho g_K a_K (V - V_K), \tag{3}$$

where the g's are the conductances and the a's contain the switching characteristics of the channels. In the steady state,

$$a_{\mathrm{Na},\infty} = a_{\mathrm{K},\infty} = \frac{1}{1+\exp[-0.25(V+25\ \mathrm{mV})]} \tag{4}$$

(see Fig. 3). The sodium channel is assumed to relax to its steady state immediately, $a_{\mathrm{Na}}=a_{\mathrm{Na},\infty}$, but the potassium current relaxes exponentially,

$$\frac{da_{\mathrm{K}}}{dt} = -\frac{\phi}{\tau_{\mathrm{K}}}(a_{\mathrm{K}} - a_{\mathrm{K},\infty}). \tag{5}$$

The dimensionless factors ρ and ϕ contain the temperature dependence,

$$\rho = \exp\left(\frac{T-T_0}{10\,^\circ\mathrm{C}} \ln 1.3\right), \tag{6}$$

$$\phi = \exp\left(\frac{T-T_0}{10\,^\circ\mathrm{C}} \ln 3.0\right), \tag{7}$$

where the reference temperature $T_0 = 25\,^\circ$C. We here follow the model as developed by Braun *et al.*, but it is clear that for the limited temperature range studied the exponential could be replaced by a linear function for ρ and a quadratic polynomial for ϕ.

The next two currents in Eq. (1) describe the slow subthreshold oscillator proposed by Braun *et al.* [1,2,4,6]. They are given by

$$I_{sd} = \rho g_{sd} a_{sd} (V - V_{sd}), \tag{8}$$

$$I_{sr} = \rho g_{sr} a_{sr} (V - V_{sr}), \tag{9}$$

where the indices sd and sr stand for ''slow depolarization'' and ''slow repolarization.'' They are assumed to relax according to

$$\frac{da_{sd}}{dt} = -\frac{\phi}{\tau_{sd}}(a_{sd} - a_{sd,\infty}), \tag{10}$$

$$\frac{da_{sr}}{dt} = \frac{\phi}{\tau_{sr}}(-\alpha I_{sd} - \beta a_{sr}), \tag{11}$$

where

$$a_{sd,\infty} = \frac{1}{1+\exp[-0.09(V+40\ \text{mV})]}. \tag{12}$$

The model for the repolarization current differs from that for the depolarization current in that it includes an activation term that is directly related to the slow depolarizing current. This reflects the general finding that slow repolarization is often carried by potassium currents which are activated by sodium or calcium currents (for experimental evidence in peripheral cold receptors, see [10]).

The temperature dependence is controlled by the same factors ρ and ϕ as above.

Finally, the model is completed by a passive leak current,

$$I_l = g_l(V - V_l). \tag{13}$$

The values of all the parameters that appear in the above equations are

Membrane capacitance $C_M = 1$ (μF/cm^2)	
Conductances (mS/cm^2)	
$g_{Na} = 1.5$	$g_K = 2.0$
$g_{sd} = 0.25$	$g_{sr} = 0.4$
$g_l = 0.1$	
Time constants (ms)	
$\tau_K = 2.0$	
$\tau_{sd} = 10$	$\tau_{sr} = 20$
Reversal potentials (mV)	
$V_{Na} = V_{sd} = 50$	
$V_K = V_{sr} = -90$	
$V_l = -60$	

(14)

and $\alpha = 0.012$ μA and $\beta = 0.17$ (dimensionless). For the simulations shown in Fig. 1 white noise is added to Eq. (1).

Typical time series for different temperatures are shown in Fig. 4. For low temperatures the time series consists of sharp spikes reaching to high voltage followed by lower and less pronounced secondary peaks. For high temperatures there are still sharp spikes but their amplitude is lower and the interspike modulations are more pronounced. The sharp peaks are due to the fast Na and K channels, the slower modulations due to the de- and repolarization currents.

The highest spikes describe the generation of a pulse on the axon and thus the time between such spikes is the physiologically relevant signal. It can be extracted as the time interval between two successive crossings of a surface of section, defined by crossing a certain voltage level in a fixed direction. The voltage level has to be higher than the one obtained in a side maximum (to avoid overcounting) and lower than the lowest maximum (so that no spikes are missed). We work with $V_{cross} = -20$ mV; the requirement $\dot{V} > 0$ then fixes the orientation of the crossing.

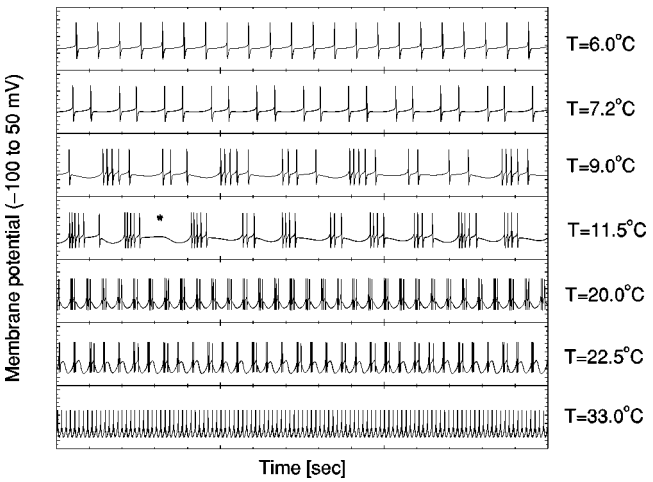

FIG. 4. Spike trains for several temperatures. The ordinates of the boxes always cover the voltage range from -100 mV to $+50$ mV, so that the absolute amplitudes can be compared. The length of the time interval shown is 15 s. At $T = 6.0\,^\circ$C and $7.2\,^\circ$C the spike activity is regular, of period 1 and 2, respectively. The trains at $T = 9.0\,^\circ$C and $11.5\,^\circ$C are irregular with narrow groups of spikes separated by long spikeless intervals (one is marked by an asterisk). At $T = 20.0\,^\circ$C the train has period 3, i.e., three spikes separated by a somewhat longer interval in which the slow oscillations of the membrane potential are visible. The train at $T = 22.5\,^\circ$C is taken from the transition region between a period 2 and a period 3 region and shows an irregular sequence of two and three spike bursts. At $T = 33.0\,^\circ$C the signal is a regular train with single spikes on top of a regular oscillation.

The numerical method used to follow a periodic orbit uses the surface of section map, the linearization in the surface of section and in the parameter, here the temperature. An orbit is first found dynamically in a temperature range where it is stable and is then followed into the region where it is unstable using PITCON, the Pittsburgh continuation program [11]. The required derivatives are found by numerical integration of the corresponding variational differential equations [12]. For completeness we give some of the relevant expressions in the Appendix.

Since there are four differential equations the monodromy is a 4×4 matrix. From the translation invariance along the trajectory one eigenvalue is 1, and the numerical linearizations reproduce this eigenvalue with high accuracy. A second eigenvalue is of the order of 1, but the other two eigenvalues turn out to be extremely small, of the order of 10^{-12} and 10^{-16}. These estimates are based on integrations of the equations of motions in 128 bit precision, but no further efforts where put into determining these eigenvalues with higher accuracy. The smallness of these two eigenvalues implies that if the dynamics becomes chaotic the attractor will have only a minimal extension in the direction of these two eigenvectors. Application of center manifold or other projection

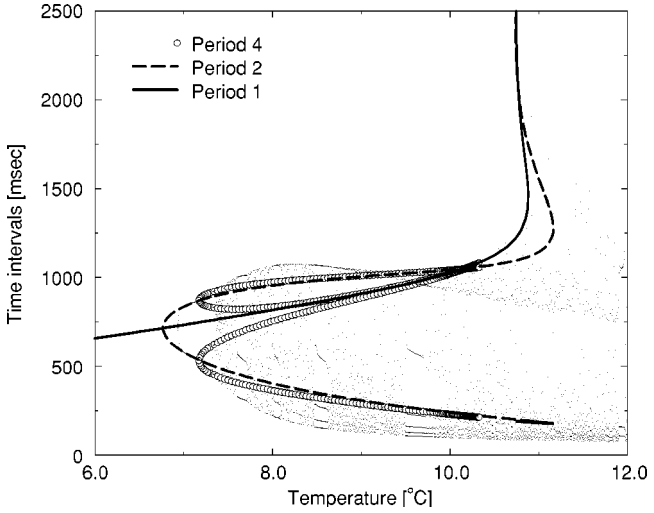

FIG. 5. The period 1, 2, and 4 orbits, superimposed on the temperature trace of Fig. 2 up to 12.0 °C. The return times of the period 1 and 2 orbits diverge near $T=10.9\,^{\circ}\mathrm{C}$ and $T=11.2\,^{\circ}\mathrm{C}$, respectively, due to an encounter with a stationary point of the system.

techniques might allow one to obtain an effective model with three degrees of freedom, but this was not attempted.

III. SWEEPING PERIOD DOUBLING TRANSITIONS

For temperatures below about 6.75 °C the thermoreceptor oscillates with a single period that increases slightly with temperature. Above that temperature a period 2 orbit takes over, then a period 4, indicative of a period doubling transition to chaos. These orbits are shown in Fig. 5. The transition from period 1 to 2 appears at $T\approx 6.7668\,^{\circ}\mathrm{C}$ (Fig. 6). In the sweeping record of Fig. 2 this transition appears at a somewhat higher temperature when going up and at a somewhat lower temperature when going down. This phenomenon was discussed earlier in connection with phase transitions [13] and is connected with the marginal stability of the orbit at the

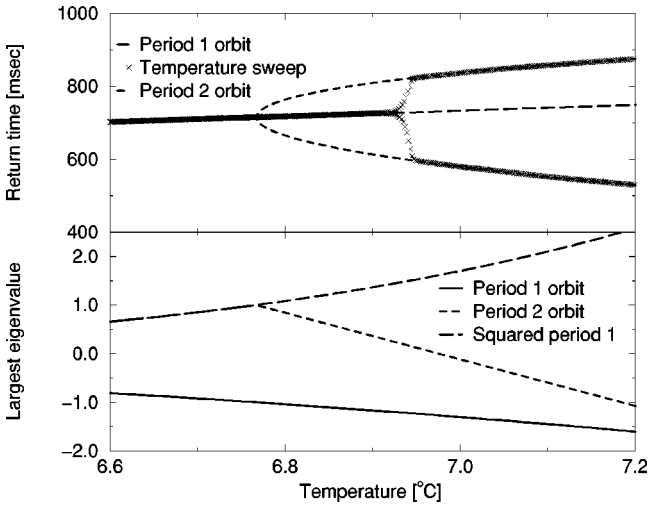

FIG. 6. Magnification of the bifurcation from period 1 to period 2. In the lower half the largest eigenvalue of the Jacobian is plotted for both orbits. The slope of the period 1 eigenvalue is $a=-1.321\,67\,^{\circ}\mathrm{C}^{-1}$.

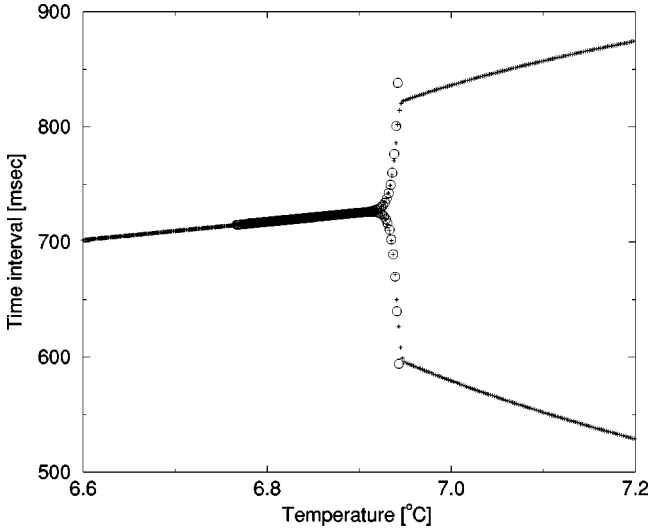

FIG. 7. Simulation of a temperature sweep through the bifurcation from period 1 to period 2. The crosses mark the data from the full calculation, the open circles the data from the approximate linear map. The temperature step ΔT is 0.001 °C.

point of bifurcation. The transition between the two states depends very much on the rate of change of the Lyapunov exponent when going through the critical region. The faster the sweep the further the trajectory will follow the old orbit before moving away.

In order to demonstrate the applicability of this model we compare the trajectories derived from a linearization of the map with the full trajectories in Fig. 7. We took an initial disturbance F_0 in the bifurcation point and computed the disturbance in the next temperature step using the iteration formula

$$F_{n+1}=-F_n(1+an\Delta T), \tag{15}$$

where a is the slope of the largest eigenvalue of the period 1 orbit with temperature (taken from Fig. 6) and ΔT is the temperature increase per spike that was used in the numerical simulations. At the point of bifurcation the eigenvalue is -1, so that $F_{n+1}=-F_n$ as is typical for a pitchfork bifurcation. Thus the absolute value of the expression in parentheses in Eq. (15) is the Lyapunov exponent of the orbit n temperature steps away from the bifurcation point. The only fit parameter for the comparison with the full simulations is the initial disturbance F_0. The two curves agree very well until the attraction of the period 2 orbit takes over.

The general scaling of the point of deviation with the sweeping speed can be estimated from the continuum version of Eq. (15). We write this as an equation of time, assuming a constant sweeping speed s, such that $\Delta T=s\Delta t$ and $n\Delta t=t$. The alternation in sign is removed with the definition $\tilde{F}_n=(-1)^nF_n$. Then

$$\frac{\tilde{F}(t+\Delta t)-\tilde{F}(t)}{\Delta t}=ast\tilde{F}(t) \tag{16}$$

and

$$\dot{\tilde{F}}=\tilde{a}t\tilde{F},\quad \tilde{a}=as, \tag{17}$$

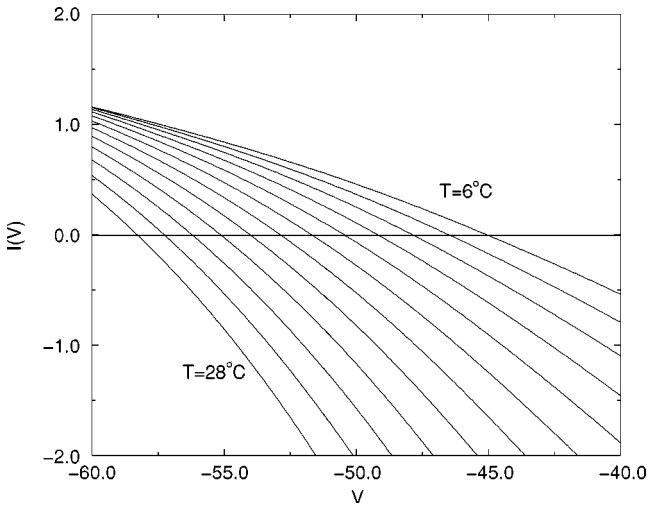

FIG. 8. The equilibrium values of the currents for different temperatures, decreasing in steps of 2 °C from left to right. Crossing the zero line indicates the presence of a stationary point. Note that the voltage values are rather low.

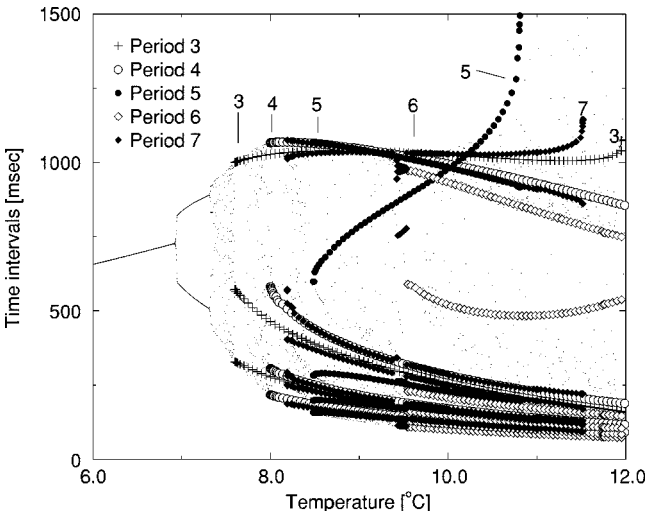

FIG. 9. Same region as Fig. 5 but with all periodic orbits that could be identified up to period 7. In the regions where most time intervals lie one notes also a higher density of periodic orbits. Similarly, there are no periodic orbits (up to this period) in the less dense region.

with solution $\tilde{F}(t)=\tilde{F}(0)\exp(\tilde{a}t^2/2)$. The time to reach a fixed threshold in F scales like $1/\sqrt{\tilde{a}}$ [note that $\tilde{a}$ as the variation of a Lyapunov exponent with time has dimensions $(\text{time})^{-2}$].

As in the period doubling scenario of the quadratic map there are windows of stable orbits beyond the accumulation point of the period doubling cascade. Some of these orbits have also been calculated and will be discussed below in connection with the accumulation of interspike intervals.

IV. DIVERGING INTERSPIKE INTERVALS

Following the period 1 orbit to higher temperatures leads to a turning point at 10.878 °C. Another turning point appears at 10.742 °C with a period time of about 2500 ms. Similarly, the period 2 orbit shows a turning point at 11.16 °C. This increase coincides with the appearance of very large interspike intervals for temperatures between 10 °C and 14 °C. As the distribution of points in Fig. 2 shows, they are rare but apparently unbounded. The left upper boundary seems to be given by the interspike intervals of the period 5 orbit, which takes off to larger intervals at slightly lower temperatures than the period 1 orbit. When following the dynamics one notes that the phase-space velocity slows down considerably in a certain part of phase space, indicating the presence of a stationary point. Indeed, such a stationary point exists for all temperatures, as we will now show.

All time derivatives in the equations of motion have to vanish at a stationary point. This fixes all currents to their equilibrium values and leaves us with a single equation for the determination of the potential V_0 at the fixed point,

$$I_{\mathrm{Na}}(V_0)+I_{\mathrm{K}}(V_0)+I_{sd}(V_0)+I_{sr}(V_0)+I_l(V_0)=0. \quad (18)$$

As Fig. 8 shows, this sum of currents crosses the zero line for all temperatures; hence the stationary point exists over the full temperature range. Between 10 °C and 15 °C the stationary point is a hyperbolic saddle, with one positive and one negative real eigenvalue and two complex conjugate ones with small positive real parts. The escape from the fixed point is thus in spirals, but since the frequency is small one has to start very close to the fixed point to detect it. As discussed in [14], the dynamics in the neighborhood of the collision with the fixed point is more complicated as there are additional saddle node and homoclinic bifurcations nearby, which also lower the critical temperature for the occurrence of infinite interspike intervals slightly.

The fixed point becomes dynamically noticeable only if the trajectories come close to the stable manifold. Thus, while it exists in the full temperature range, it seems to interfere with the dynamics only in the interval between about 10 °C and 15 °C.

Physiologically, the presence of this fixed point is rather interesting as it can cause a blocking of the sensor for some time. Note that there is more than a factor of 10 between the shortest and largest interspike intervals. Thus the response of the sensor shows a large intrinsic variability in this temperature range.

V. ACCUMULATION OF INTERSPIKE INTERVALS

Next we turn to the accumulation of interspike intervals near an almost constant lower value of about 150 ms and an upper one that decreases from about 1000 ms to 650 ms for temperatures between 10 °C and 14 °C. We will give two explanations of this behavior.

The first is a statistical analysis of the interspike intervals that appear in periodic orbits. Fig. 9 shows the orbits with periods up to 7 in the temperature range up to 12 °C. Most of the branches cluster in the lower fourth of the time scale, some branches lie above about 800 ms, and only a few visit the intermediate region. To connect this distribution of interspike intervals in periodic trajectories to the invariant ergodic density, we have to appeal to periodic orbit theory [15,16]. The trajectories of a dynamical system fill up most of the phase space and their densities and instabilities can be

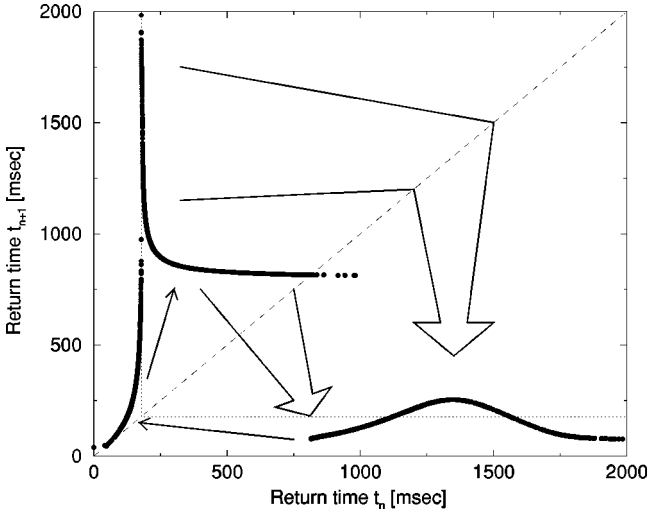

FIG. 10. First return map at $T=11\,^{\circ}\mathrm{C}$. The large arrows indicate the order of the mapping by the three branches.

used to characterize the invariant phase-space density. Specifically, if there is not much variation in the instability of orbits (as is the case here), the density of periodic points directly indicates the invariant density. The accumulation of periodic points in the two mentioned areas (see Fig. 9) thus is direct evidence for an increased invariant density.

The second explanation for the gap in the density of interspike intervals is based on the first return map, t_{n+1} vs t_n, a typical example of which is shown in Fig. 10 for $T=11\,^{\circ}\mathrm{C}$. In the return map three branches are discernible, one starting near the diagonal and diverging near 175 ms, a second part starting near the divergence and leveling off near about 1000 ms, and a third part that maps large interspike intervals to short ones. Note that the last two overlap. This ambiguity is resolved by the observation that large time intervals induced by branch 1 are mapped by branch 2 and large time intervals derived from branch 2 are mapped by branch 3.

Essential for the spike accumulation is the second branch, which has a flat plateau in the time interval 250 to 1000 ms. Should any interspike time fall in this interval, it is followed by another of about 820 ms and then one with about 75 ms. This large interval thus gets mapped on a much smaller one in one time step. Similarly, the probability of entering this interval requires special precursor interspike intervals. As a result, the invariant density has high values near the boundary and very low ones in the middle. A similar effect is familiar from the quadratic map, where also the density accumulates at the boundaries because of the flat derivative at the maximum. Here it is more pronounced since the map is rather flat over most of the interval.

VI. AUTORESONANCES

For higher temperatures the system shows limit cycle dynamics with periods decreasing in steps of 1 from period 4 near $T=15\,^{\circ}\mathrm{C}$ to period 1 for $T>28\,^{\circ}\mathrm{C}$. The transition region between periods $n+1$ and n is narrow, but full of complicated dynamical behavior. As we will show now the origin of this behavior is what might be called an autoresonance between fast and slow currents.

As mentioned, the dynamics of the voltage across the membrane is controlled by two pairs of currents, the fast channels that make the spikes and a slower channel for the polarizations across the membrane. The individual periods can be estimated from the limit cycles in the spiking subsystem,

$$C_M\dot{V}=-I_{\mathrm{Na}}-I_{\mathrm{K}}-I_l-I_{dr}, \tag{19}$$

and in the slow oscillating subsystem,

$$C_M\dot{V}=-I_{sd}-I_{sr}-I_l, \tag{20}$$

where the currents and numerical constants for the full system are used. An additional current has to be added to drive the spiking system. The periods can again be obtained from a surface of section, with a lowered crossing voltage V_{cross} for the slow oscillator. The period of both oscillators in isolation decreases with increasing temperature, but it decreases faster for the slower process.

In this approximation of two independent oscillators the slow one modifies the potential difference and thus the level at which the firing of the fast oscillator is triggered. Thus in each polarization period there is a time window near the maximum of the depolarization where spike generation is very likely (resulting in a sequence of narrowly spaced spikes), while in passing through the minimum of the oscillation spike generation is mostly suppressed. The width of this time window and the period time of the spike generator essentially determine the number of spikes in one oscillation period. When both resonators are combined, the nonlinear interactions cause the spike generation to lock exactly into some periodic limit cycle. To test this resonance picture we have calculated the total period of the spike trains in the various temperature intervals and compared it with the period of the polarization system (20). As shown in Fig. 11 the total period and that from the polarization system are very close, and the small deviations can be attributed to interaction effects. Since the two oscillators that are in resonance are both part of the system we call this effect an autoresonance.

The resonance picture suggests labeling the states in the temperature regions marked by E, F, and G in Fig. 2 as 3:1, 2:1, and 1:1 resonances, respectively, since there are 3, 2, and 1 spikes within one period of the polarization system. More generally, we would define an $n{:}m$ resonance if n spikes fit into m intervals of the polarization current.

The standard model of interacting resonators and mode locking is the circle map [17]. If the coupling between resonators is weak there is a hierarchy of resonances whose width is determined by their order $n{:}m$. The present model, however, seems to be far from the weak coupling behavior, since the $n{:}1$ resonances are very prominent and leave only small parameter intervals for other resonances, and also since in the regions between these prominent resonances others seem to coexist.

Between the main $n{:}1$ resonances the behavior is more complicated, with many transitions in a tiny interval. In particular, this is the case in the transition region between the 2:1 resonance and the 1:1 resonance, near a temperature of $28\,^{\circ}\mathrm{C}$. As the temperature increases, the size of the time

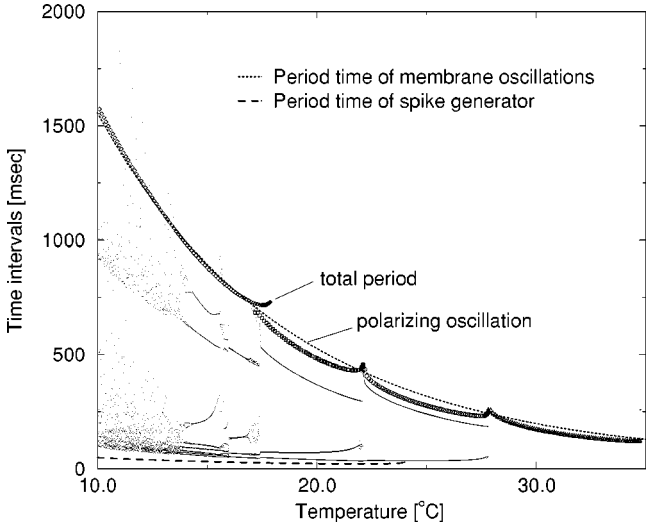

FIG. 11. Resonances between the polarization/depolarization currents and the spike generator in the interval between 10 °C and 35 °C. As the temperature increases the period changes from 4 to 3, then from 3 to 2, and then to 1. Between these wide and distinguished intervals there are small regions with more complicated dynamics. The continuous lines give the period of the polarization system and of the sum of n consecutive time intervals in the period n intervals.

window decreases, but is still too large for a single spike. Thus, the system combines two periods of the slow oscillator and fits in three spikes, creating a 3:2 resonance. This process continues, giving rise to 4:3,5:4,6:5, . . . resonances, as shown in the magnifications in Fig. 12 and Fig. 13.

VII. CONCLUDING REMARKS

Application of methods from dynamical system theory has helped to understand many details in the dynamics of a thermoreceptor. The system shows a rich variety of dynamical responses to temperature changes. The accumulation of

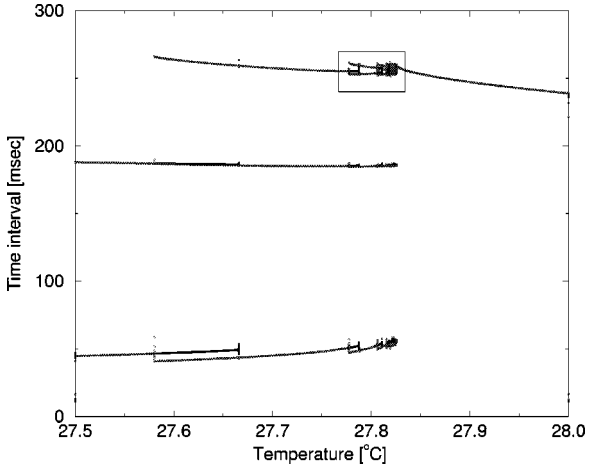

FIG. 12. Magnification of the transition region between the period 1 and period 2 regimes. To the left is the 2:1 resonance, to the right the 1:1 resonance. In between there is a period 3 state which corresponds to a 3:2 resonance. The small box indicated in the upper middle is magnified in Fig. 13.

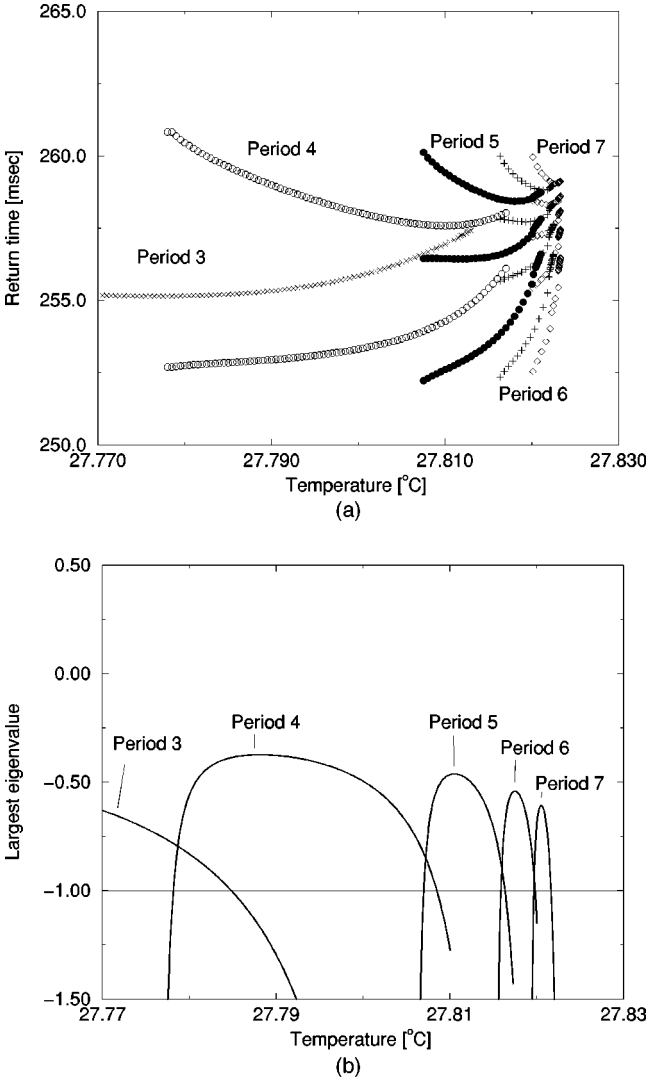

FIG. 13. Magnification of the box in Fig. 12. The periodic orbits with periods n up to 7 indicated correspond to $n:(n-1)$ resonances. The Lyapunov exponents in the lower frame show that stable resonances coexist, indicating that in relation to the circle map one is in the strong perturbation region.

spike intervals, the blocking due to the fixed point, and the period decreasing transitions at higher temperatures should be features robust enough to survive slight modifications in the model and the addition of weak noise. The effects of noise on the intermittency near the divergence of the interspike interval have already been studied by Feudel *et al.* [14]. The sequence of higher periodic resonances between the n:1 resonances presumably is less observable because of the tiny widths of the parameter intervals. It would be nice to have further experiments testing the features of the model; in particular, it seems worthwhile to look for parameters that allow manipulation of the location and stability of the stationary point in phase space and thus study of the conditions under which the sensor can be blocked.

The autoresonance between the fast and slow ion channels is also of interest. Since there are many channels with similar characteristics crossing a membrane it seems worthwhile to check other membrane models for autoresonance behavior as a function of some external parameter. For instance, it might also appear in the response of isolated and connected recep-

tors to external periodic driving, as in the studies on paddle fish [18].

The rather complicated response of the sensor as a function of temperature raises the question of just how the temperature is encoded in the spike trains, especially as the firing rate vs temperature relation is not monotonic and therefore cannot provide unambiguous information. One possible scenario is that the spike trains are integrated over some time interval. Assuming that synaptic transduction becomes more effective with an increased number of short intervals within a given group of impulses, the fibers would sense ''coldness'' when the temperature is lowered in the range above 10 °C. Lower skin temperatures are generally perceived as rather strange sensations, and may be painful. It is still unclear whether this is due to additional activation of low temperature or unspecific receptors. Perhaps also the transition to chaotic patterns and transient blocking of the discharge might contribute to such strange sensations. Further experiments are needed to clarify this issue.

ACKNOWLEDGMENT

We have greatly benefited from discussions with B. Lani-Wayda on the mathematical aspects of the model.

APPENDIX: LINEARIZATIONS AND SURFACES OF SECTIONS

In this Appendix we give some details for the calculation of the entries for the surface of section maps. To simplify the notation, let $x_1, \ldots, x_4$ be the four variables and $f_i(x_j, \lambda)$ be the right hand sides of the differential equations; they depend on all variables and a parameter λ, here the temperature.

The monodromy matrix M for linearizations in initial conditions solves

$$\dot{M}_{ij} = \sum_k \frac{\partial f_i}{\partial x_k} M_{kj} \tag{A1}$$

with initial conditions $M_{ij} = \delta_{ij}$. When integrated along a periodic orbit, this matrix has one eigenvalue 1 with eigenvector equal to the phase-space velocity, the right hand side of the differential equation.

Variations of parameters can be calculated in a similar fashion, the relevant differential equations being

$$\frac{d}{dt}\left(\frac{\partial x_i}{\partial \lambda}\right) = \sum_k \frac{\partial f_i}{\partial x_k}\frac{\partial x_k}{\partial \lambda} + \frac{\partial f_i}{\partial \lambda}. \tag{A2}$$

The reduced map from the surface of section back to the surface requires that the final points also come to lie in the surface of section. Going around a periodic orbit, a perturbation starting in the surface of section will not be mapped back into the surface of section, it will come to lie slightly before or after the surface of section. Therefore, the perturbed trajectory has to be integrated for a slightly changed time interval. Since all changes are infinitesimal, this modification can be accomplished by linear transformation with the phase-space velocity. Specifically, let the surface of section be defined by $x_1 = c$ and $\dot{x}_1 > 0$, and let δx_j be a variation in a direction in the surface of section. After one period of a periodic orbit it will be mapped by M into a variation

$$\delta x_i' = M_{ij}\delta x_j, \tag{A3}$$

where typically $\delta x_1' \neq 0$. Following the trajectory for a small time δt will change the point into

$$\delta x_i'' = M_{ij}\delta x_j + \delta t f_i. \tag{A4}$$

The requirement $\delta x_1'' = 0$ fixes

$$\delta t = -\frac{M_{1j}}{f_1}\delta x_j. \tag{A5}$$

Combining this reasoning for all possible variations in the surface of section allows one to define a reduced monodromy matrix

$$m_{ij} = M_{ij} - \frac{f_i}{f_1} M_{1j} \tag{A6}$$

that describes the mapping of deviations in the surface of section. In this reduced map the indices run through $i = 2,3,4$ since the surface of section coordinate is $i = 1$. Similar transformations are applied to the variations in parameter (which also change the period of the orbit).

[1] H. A. Braun, M. Wissing, K. Schäfer, and M. C. Hirsch, Nature (London) **367**, 270 (1994).

[2] K. Schäfer, H. A. Braun, R. C. Peters, and F. Bretschneider, Pflügers Arch. **429**, 378 (1995); H. A. Braun, K. Schäfer, K. Voigt, R. Peters, F. Bretschneider, X. Pei, L. Wilkens, and F. Moss, J. Comput. Neurosci **4**, 335 (1997).

[3] H. A. Braun, H. Bade, and H. Hensel, Pflügers Arch. **386**, 1 (1980).

[4] H. A. Braun, M. Dewald, K. Schäfer, K. Voigt, X. Pei, and F. Moss, J. Comput. Neurosci. **7**, 17 (1999).

[5] X. Pei and F. Moss, Nature (London) **379**, 618 (1996); X. Pei, K. Dolan, F. Moss, and Y.-C. Lai, Chaos **8**, 853 (1998).

[6] H. A. Braun, M. T. Huber, M. Dewald, K. Schäfer, and K. Voigt, Int. J. Bifurcation Chaos Appl. Sci. Eng. **8**, 881 (1998).

[7] E. Ott, *Chaos in Dynamical Systems* (Cambridge University Press, Cambridge, England, 1993).

[8] H. G. Schuster, *Deterministic Chaos* (VCH-Wiley Publishers, Weinheim, 1995).

[9] J. Rinzel and B. Ermentrout, *Methods in Neuronal Modeling*, 2nd ed., edited by C. Koch and I. Segev (MIT Press, Cambridge, MA, 1998), p. 251.

[10] K. Schäfer, H. A. Braun, and L. Rempe, Experientia **47**, 47 (1991).

[11] W. C. Rheinboldt and J. Burkardt, Pittsburgh program, version 6.1, University of Pittsburgh, 1991.

[12] H. Kawakami, IEEE Trans. Circuits Syst. **31**, 248 (1984).

[13] S. Grossmann and A. S. Mikhailov, Z. Phys. B: Condens. Matter **78**, 1 (1990).

[14] U. Feudel, A. Neiman, X. Pei, W. Wojtenek, H. Braun, M. Huber, and F. Moss, Chaos **10**, 231 (2000).

[15] P. Cvitanović, Physica D **83**, 109 (1995).
[16] P. Cvitanović and B. Eckhardt, J. Phys. A **24**, 4335 (1991).
[17] T. Bohr, P. Bak, and M. H. Jensen, Phys. Rev. A **30**, 1960 (1984).
[18] A. Neiman, X. Pei, D. Russel, W. Wojtenek, L. Wilkens, F. Moss, H. A. Braun, M. T. Huber, and K. Voigt, Phys. Rev. Lett. **82**, 660 (1999).